Dynamics of Completely Unfolded and Native Proteins through Solid-State Nanopores as a Function of Electric Driving Force

Abdelghani Oukhaled,[†,⊥] Benjamin Cressiot,[†] Laurent Bacri,[†] Manuela Pastoriza-Gallego,[†] Jean-Michel Betton,[‡] Eric Bourhis,[⊥] Ralf Jede,[∥] Jacques Gierak,[⊥] Loïc Auvray,[§] and Juan Pelta[†,*]

[†]LAMBE UMR CNRS 8587, Université d'Evry et de Cergy-Pontoise, France, [‡]Unité de Biochimie Structurale, Institut Pasteur, France, [§]Matière et Systèmes Complexes, UMR 7057, Université Paris Diderot, France, [⊥]LPN/CNRS, Marcoussis, France, and [∥]RAITH GmbH, Hauert 18, Technologiepark, D-44227 Dortmund, Germany

ABSTRACT We report experimentally the dynamic properties of the entry and transport of unfolded and native proteins through a solid-state nanopore as a function of applied voltage, and we discuss the experimental data obtained as compared to theory. We show an exponential increase in the event frequency of current blockades and an exponential decrease in transport times as a function of the electric driving force. The normalized current blockage ratio remains constant or decreases for folded or unfolded proteins, respectively, as a function of the transmembrane potential. The unfolded protein is stretched under the electric driving force. The dwell time of native compact proteins in the pore is almost 1 order of magnitude longer than that of unfolded proteins, and the event frequency for both protein conformations is low. We discuss the possible phenomena hindering the transport of proteins through the pores, which could explain these anomalous dynamics, in particular, electro-osmotic counterflow and protein adsorption on the nanopore wall.

KEYWORDS: solid-state nanopore · focused ion beam · protein transport · protein unfolding · anomalous transport

The electrically driven manipulation of single biological or synthetic macromolecules by transport across a nanopore is now widely used[1−6] and has many important potential applications,[7,8] particularly for ultrafast DNA sequencing.[7] In most cases, an applied electric field drives a macromolecule into the nanopore, inducing a transient blockade of electrical current and a measurable increase in electrical resistance.[9] The current blockade duration and rate depend on the size and conformation of the passing macromolecule, the diameter, length, and protein pores or solid-state pores and the interaction between the molecule and the pore walls. Two types of nanopore are used in practice: natural or modified protein channels[4,10] or artificial nanopores drilled by different techniques through solid-state semiconductor[1,11] or polymer membranes.[12]

Inspired by the biological example of protein transport through the translocon machinery,[13] we have spent several years studying the use of a protein pore, α-hemolysin, as a conformation filter for completely or partially unfolded proteins.[14] We have recently studied the dynamics of unfolded proteins through an aerolysin channel.[15] Toxin channels are very good sensors to probe the conformation of passing polypeptide chains because their diameter is very small.[15−19] On the other hand, protein channels are slightly sensitive to denaturing agents.[15,20,21] Solid-state nanopores offer the advantage of customized pore diameters, and they exhibit high chemical resistance to denaturing agents.[22]

Nanofabricated pores have already been used to detect proteins, in their native state.[22−27] In these studies, the pore diameter is much larger than the protein diameter, but the experiments are sensitive to the relative charge and size of the proteins. In one case, protein transport through the nanopores has been proven using a luminescence assay.[23] An unexplained feature of these early experiments is that the dwell time of proteins inside the pores is strikingly long, on the order of a few hundred microseconds, 2 orders of magnitude larger than expected. Solid-state nanopores have also been used to study pore−DNA interactions,[28] protein−protein interactions, in particular antigen−antibody binding.[25,26] They have shown that the ionic current blockade can provide information about the size and stoichiometry of the complex antigen−antibody. In this last experiment, the observed protein current blockade durations are also many orders of magnitude longer than the expected electrophoretic

* Address correspondence to juan.pelta@bio.u-cergy.fr.

Received for review December 15, 2010 and accepted April 8, 2011.

Published online April 08, 2011
10.1021/nn1034795

transport times (pH close to the pI). Recently, new experiments have been performed to study protein translocation for different proteins.[27,29] The authors also find that the transport event durations are many orders of magnitude longer than the electrophoretic transport time. They suggest that the protein engages in repeated adsorption/desorption processes at the pore and nanotube walls. Recent data suggest that proteins which have dimensions similar to or larger than the pore diameter do not translocate, and smaller proteins can apparently translocate in a folded conformation.[30] Solid-state nanopores have also been used to study folded, partially unfolded, and fully unfolded proteins (bovine lactoglobulin) in three different states corresponding to three concentrations of denaturing agent, urea.[22] These states can be distinguished by the depth and duration of the measured current blockades. The dynamics of the translocation are also found to be anomalously slow, a fact which the authors suggest could be associated with the disorder of electric charges along the protein sequence. As shown recently in interesting experiments that directly probe the electrokinetic effects occurring in nanopores, electro-osmotic flow due to the surface charge of the pores may reverse the electrophoretic transport of proteins.[31]

To date, there is only an incomplete understanding of the dynamics of native and unfolded proteins through solid-state nanopores as a function of the applied voltage. We wish to use solid-state nanopores to study protein unfolding at the single-molecule level. However, the first stage is to control the physical mechanisms of protein translocation through a solid-state nanopore as a function of the electric driving force. To get a better insight, we compare folded and unfolded proteins and systematically vary the applied electrical force between 25 and 250 mV. In our experiments, we use a protein model for the translocation and for the protein folding: this is the recombinant maltose binding protein (MBP) or MalE.[32] The role of this periplasmic protein is to transport maltose inside the bacteria. In order to compare data obtained previously with protein (MalE) transport through protein pores, α-hemolysin,[14,17] aerolysin,[15] and the dynamics of MalE through a solid-stade nanopore in a silicon nitride membrane, we have used the same order of protein concentration. MalE is completely unfolded in the presence of guanidium chloride (1.44 M). We mainly probe a regime where the pore diameter (20 nm) is larger than the size of the proteins. Its native shape is ellipsoidal[33] with overall dimensions of $3 \times 4 \times 6.5$ nm^3. The protein, MalE, is composed of 51 acidic residues (24 Asp + 27 Glu) and 43 basic residues (37 Lys + 6 Arg), uniformly distributed along the primary sequence. Its pI is 5.2; thus the protein is negatively charged at pH 7.5, and the protein net charge is −8e. From the 3D structure, there is no visible cluster of charged residues. We analyze the primary structure of MalE (or MBP) using the SAPS program (www.ebi.ac.uk/Tools/saps, developed by S. Karlin) to evaluate the presence of charge cluster or other compositional amino acid biases.[34] This analysis did reveal any positive or negative charge clusters; therefore, we assumed that charged residues are also uniformly distributed in the unfolded conformation. The unfolded MalE protein is treated as a uniformly distributed negatively charged polymer. In order to check that the protein is inside the nanopore and confirm the pore diameter, in relation with the level of the current blockade, we performed another experiment where the pore diameter (4 nm) is smaller than the unfolded protein size (a new recombinant double MBP protein consisting of two tandem MalE sequences and whose diameter is at least 12 nm for an unfolded state).

We observed that the ionic current increases in the presence of the denaturing agent, guanidium chloride. The current blockade increases linearly as the applied voltage increases. The normalized current blockage remains constant or decreases for folded or unfolded proteins, respectively, as a function of the transmembrane potential. We analyze transport parameters: frequency of current blockades, activation energy, effective charge of the protein, and dwell time. The blockade rate is described by a Van't Hoff−Arrhenius law. We show that the confined protein chain dynamics are associated with a free-energy barrier. The dwell time decreases exponentially as a function of voltage. The capture rate of native and unfolded proteins is low, and their dwell times are very long. We discuss these anomalous dynamics inside the solid-state nanopore.

RESULTS AND DISCUSSION

Analysis of the Currents Blockade. We first present results obtained with native MBP proteins. After the addition of native proteins in the *cis* (negative) compartment, deep current blockades are observed (Figure 1c). A detail of a current trace is shown in Figure 1c (top panel). The baseline of the current remains stable during the acquisition, often made during several minutes. A typical current blockade is shown at high resolution in Figure 1c (bottom panel). In the inset of Figure 1d, we observe two types of events: short rectangular events and longer events with an enhancement portion. Each corresponds to a single protein inside the pore and probably to two proteins translocating, respectively. This inset allows us to define the main characteristics of the current trace: blockade duration T_t, related to the dwell of a protein in the pore; inter-event time T_i, related to the frequency of blockades; mean open pore current $\langle I_o \rangle$ (associated with the pore conductance) and mean blockade pore current $\langle I_b \rangle$. Figure 1d shows a plot of the current blockade DI = $\langle I_o \rangle - \langle I_b \rangle$ *versus* the dwell time T_t exhibiting the

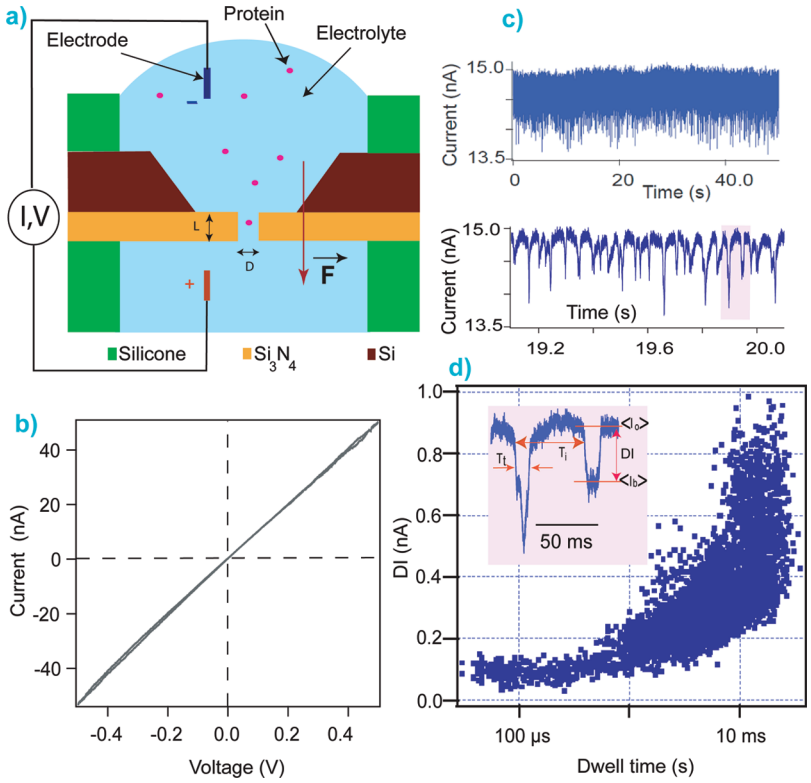

Figure 1. Direct focused ion beam (FIB) nanopore fabrication for the detection of native and unfolded proteins. (a) Experimental setup for single-molecule measurements with a nanopore sensor. A negatively charged protein molecule is driven by an electric field through 20 nm aperture of a solid-state Si_3N_4 membrane. Both reservoirs are filled with an aqueous buffer solution (1 M KCl, 10 mM Tris, pH 7.5). (b) *I*−*V* curve characterization of a solid-state nanopore in 1 M KCl; the apparent nanopore diameter is 20 nm. The linear fit yields a conductance of 103 ± 3 nA/V. (c) Detail of a current trace recording in the presence of native MBP protein. Individual events are shown with increased time resolution (bottom). (d) Event scatter plot of dwell time *versus* current blockade. The inset shows two successive individual events, with corresponding dwell time T_t, inter-event time T_i, mean current level of the empty pore $\langle I_o \rangle$, mean blockade pore current $\langle I_b \rangle$, and current blockade DI = $\langle I_o \rangle - \langle I_b \rangle$; we use the maximum current blockade during each event for data analysis. The protein concentration is 0.78 μM, and the transmembrane potential is 100 mV.

classical correlation between deep and long blockades. We have systematically examined the normalized conductance variation DG *versus* dwell time scatter plots for all applied voltages (Figure 2). We observe that the dwell time and the normalized conductance variation of the native MBP proteins (Figure 2a) are larger than those of the unfolded proteins (Figure 2b). The effect is also observed when we increase the applied voltage to 200 mV (Figure 2c,d). The current blockade could be associated with the difference in occupied volume either by a globular protein inside the pore or by the one occupied by a completely unfolded protein. We further analyze the behavior of dwell times of native and unfolded proteins in terms of electrical charge distribution, hydrodynamic interactions, and drag forces. We measure the current blockade $\langle I_o \rangle - \langle I_b \rangle$ (Figure 3a) from the full current trace histogram shown in Figure 3b. We observe two distinct populations: the first one corresponds to the noisy ionic current of the "empty pore", the second one to the presence of the proteins inside the pore (Figure 3b). We check that the mean of the current blockade increases linearly as a function of the applied voltage from 50 to 200 mV (Figure 3c) for two different protein concentrations and for native and unfolded proteins (data not shown). The blockade frequency of unfolded proteins is, however, much smaller, and significant statistics are only obtained when using larger concentrations. We compare, in Figure 3d, the blocking ratio of folded and unfolded proteins. The normalized currents blockade is defined as $(\langle I_o \rangle - \langle I_b \rangle)/\langle I_o \rangle$ and the percentage of the normalized currents blockade I_B (%) as $(\langle I_o \rangle - \langle I_b \rangle)/\langle I_o \rangle \times 100$; we observe that normalized current is independent of the voltage for native proteins. This result suggests that the blockades observed are indeed due to the presence of the proteins inside the pore and not at the pore entry. We notice that the normalized current blockade remains constant for folded proteins as a function of the transmembrane potential while it decreases for unfolded proteins. This probably means that the conformations of the flexible unfolded proteins inside the pore depend on the applied electric field. Furthermore, this suggests that the volume occupied by the unfolded chains in the pore is smaller than that of folded chains, and that it decreases as the voltage increases. All of these considerations let us

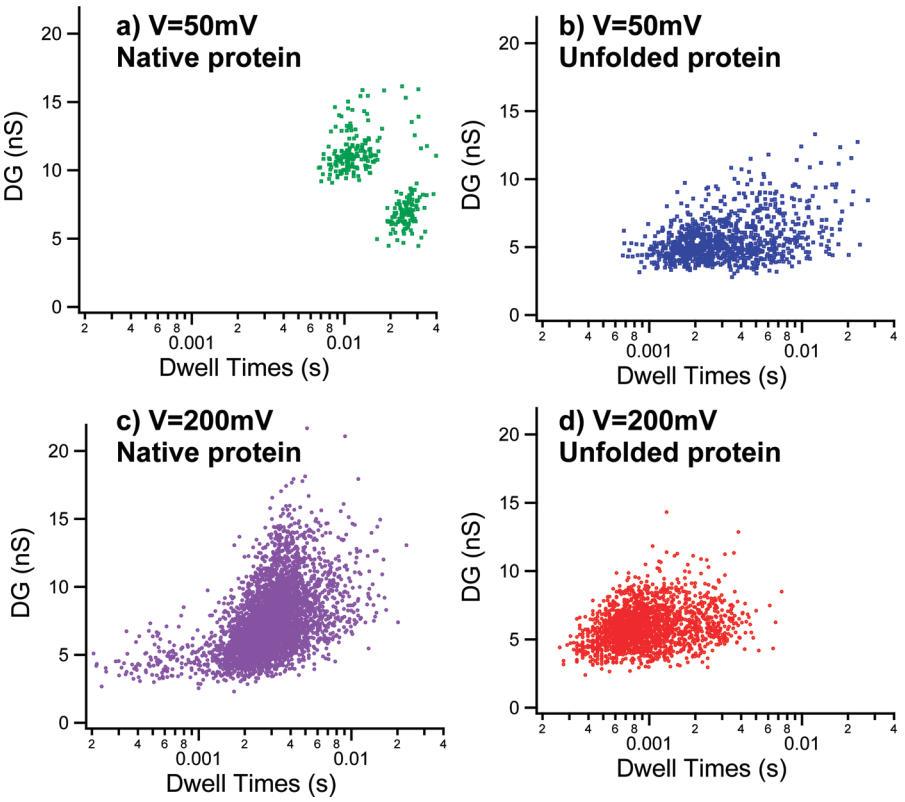

Figure 2. Nanopore as a sensor for the detection of native and unfolded protein conformation. Scatter plot of normalized conductance variation DG *versus* the dwell time at different applied voltages for native (left) and unfolded (right) MBP proteins. The conductance is normalized by taking into account the change of the conductivity with 1.44 M or without the guanidium-HCl in the buffer solution.

presume that unfolded polypeptide chains are progressively stretched as the applied force increases. We make a more quantitative analysis by comparing the value of the normalized current blockade, $I_B = (\langle I_o\rangle - \langle I_b\rangle)/\langle I_o\rangle$, to its theoretical value, which is to a first approximation the volume occupied by the protein inside the pore. For the native protein assumed to be ellipsoidal $V_{MBP}/V_{pore} = (4/3\pi abc)/(\pi r_{pore}^2 L_{pore})$, with a, b, and c being the MBP dimensions 3, 4, and 6.5 nm, respectively, and by considering a cylindrical nanopore shape of radius r_{pore} and length L_{pore}, V_{MBP}/V_{pore} = 3.5%, we obtain $I_B = (\langle I_o\rangle - \langle I_b\rangle)/\langle I_o\rangle = 4.5 \pm 0.7\%$ (Figure 3d). Both values are indeed very close. For the unfolded protein, we choose the reference geometry to be that of the fully extended molecule. We estimate the lower blocking ratio with a cylinder of radius $r_{mono} = 0.33$ nm (radius of an amino acid) spanning the whole length of the pore. In this case, $V_{MBP}/V_{pore} = r_{mono}^2/r_{pore}^2 = 0.1\%$. A more realistic estimation is to take into account the thickness of the chain, 0.66 nm; we find $V_{MBP}/V_{pore} = r_{mono}^2/r_{pore}^2 = 0.4\%$. An excluded volume chain will be evaluated by taking into account the Kuhn length; this length is the statistical segment for unfolded protein, $t_{chain} = 1.32$ nm,[35] and we find $V_{MBP}/V_{pore} = 1.69\%$. The largest experimental value of $I_B = (\langle I_o\rangle - \langle I_b\rangle)/\langle I_o\rangle$ obtained at the smallest voltage (50 mV) is $I_B = 1.8 \pm 0.2\%$, and the smallest experimental value I_B obtained at the highest voltage (250 mV) is $I_B = 0.6 \pm 0.1\%$. The theoretical estimate yields the right order of magnitude of the observed values. We deduce from the difference between both values that the chain is stretched under the electric driving force.

Capture Rate of Native and Unfolded Proteins. We use two values of protein concentration in the native or unfolded state. We check in each case that the mean blockade frequency (derived from the blockade histograms shown in Figure 4a,b) is proportional to protein concentration. The relevant variable is the capture rate, R, defined as the frequency per unit of concentration. From the inter-event duration histogram, we observe that the blockade current frequency increases as the applied voltage increases from 50 mV (Figure 4a) to 200 mV (Figure 4c).

The capture rate R as a function of the voltage is, in general, described by a Van't Hoff–Arrhenius law, $R = R_0\exp(|V|/V_0)$, where $R_0 \propto f^*\exp(-U^*/k_BT)$ is the zero voltage capture rate controlled by an activation barrier U^* (f^* is a frequency factor) of entropic and electrostatic origin. The ratio $|V|/V_0 = (zeV)/k_BT$ is a barrier reduction factor due to the applied voltage V, acting on ze, the effective electric charge of the molecule, where z is the magnitude of the effective total number of elementary charges on the protein, e is the magnitude of the elementary charge, and k_BT is the thermal energy.[36]

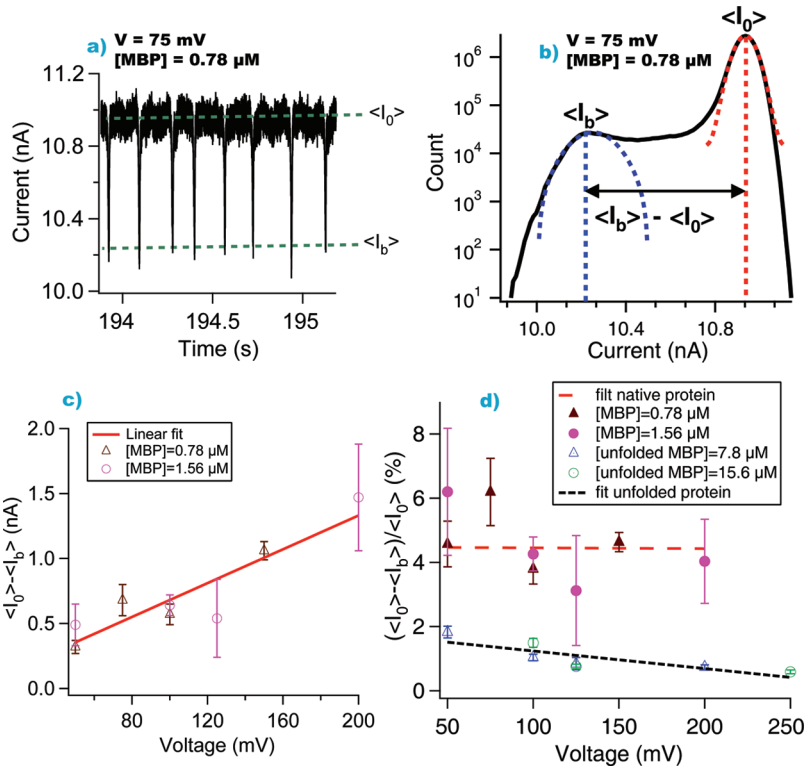

Figure 3. Comparison of the current blockade ratio of native and unfolded proteins as a function of applied voltage. (a) Detail of current trace recording at 75 mV showing the mean current empty pore $\langle I_o \rangle$ and the mean blockade pore current $\langle I_b \rangle$. (b) Corresponding histogram of the full current trace used to define $\langle I_o \rangle$ and $\langle I_b \rangle$ from the mean of the Gaussian fitted to the first and second peak. (c) Evolution of current blockade $\langle I_o \rangle - \langle I_b \rangle$ as a function of applied voltage. The solid line is a linear fit whose equation is $f(V) = bV + a$, with $a = 0.03 \pm 0.14$ nA, $b = 0.006 \pm 0.001$ nA mV^{-1}. (d) Evolution of the normalized blockade ratio (%) $(\langle I_o \rangle - \langle I_b \rangle)/\langle I_o \rangle \times 100$ as a function of applied voltage. Dotted lines are linear fits of equation $f(V) = bV + a$. We obtain $a = 4.5 \pm 0.5\%$, $b = -0.00026 \pm 0.0001\%$ mV^{-1} for native proteins; and $a = 1.8 \pm 0.26\%$, $b = 0.0054 \pm 0.002\%$ mV^{-1} for unfolded proteins.

The potential V_0 ($V_0 = (k_BT)/(ze)$) corresponds to the necessary applied potential to allow a charged protein to overcome the Brownian motion.

Frequency data are well-described by an exponential fit of the equation $f = f_0 \exp(|V|/V_0)$ in the whole range of potentials for folded proteins and at low voltage for unfolded ones. We obtain $f_0 = 5.5 \pm 0.5$ Hz (at $c = 1.56$ μM), $R_0 = 5.9 \times 10^{-21}$ m^3/s, $V_0 = 56.4 \pm 0.5$ mV, and $z = (k_BT/e)(1/V_0) = 0.45 \pm 0.01$ for folded proteins and $f_0 = 0.14 \pm 0.01$ Hz (at $c = 15.6$ μM), $R_0 = 5.9 \times 10^{-23}$ m^3/s, $V_0 = 45 \pm 0.5$ mV, $z = (k_BT/e)(1/V_0) = 0.6 \pm 0.01$ for unfolded proteins. These values are close to the effective charge found for unfolded MBP proteins through the α-hemolysin pore ($z = 0.6$).[14] In order to obtain an estimate of the activation energy (U^*) for the native protein, the frequency factor (f^*) is estimated by a barrier penetration calculation $f^* \cong CD_{diff}A_{pore}/L_{pore}$, where $C \cong 9.4 \times 10^{20}$ molecules/m^3 is the bulk concentration of native MBP protein (corresponding to $c = 1.56$ μM), $D_{diff} \cong 10^{-10}$ m^2/s its diffusion coefficient, $A_{pore} \cong \pi 10^{-16}$ m^2 is the cross-sectional area of the pore, and $L_{pore} = 30 \times 10^{-9}$ m the pore length, we calculate $U^* \cong 7.4k_BT$. A similar analysis yields $U^* \cong 10.4k_BT$ for the MBP proteins in their unfolded state. This estimated value is surprisingly high in comparison to unfolded protein entry through narrow protein pores which have smaller diameters than a solid-state nanopore. We have found $U^* \cong 4k_BT$[15] for unfolded MBP proteins passing through an aerolysin pore, and a lower value, $U^* \cong 2k_BT$, with an α-hemolysin pore.[14] The activation energy is high in the case of solid-state nanopore, and this could be due to hydrodynamic effect as observed previously by Storm *et al.*[37] There is an essential difference between solid-state nanopore and protein nanopore. The friction outside the pore is dominant. The friction is proportional to the size of the protein (hydrodynamic radius). For the unfolded protein (MBP), the size of the protein increases by a factor 2 in comparison to native conformation, consequently the friction increases. This is a possible reason for the difference in term of activation energy between the two chain conformations.

As Si_3N_4 membranes are negatively charged, one might think, as explained by several groups,[31,38,39] that electro-osmotic counterflow could slow down and hinder the penetration of the negatively charged DNA[38,39] or proteins[31] into the pores. However, if the electro-osmotic effects were dominant, one would expect that the capture would decrease when increasing the applied electric field. The nanopore (SiN) is highly

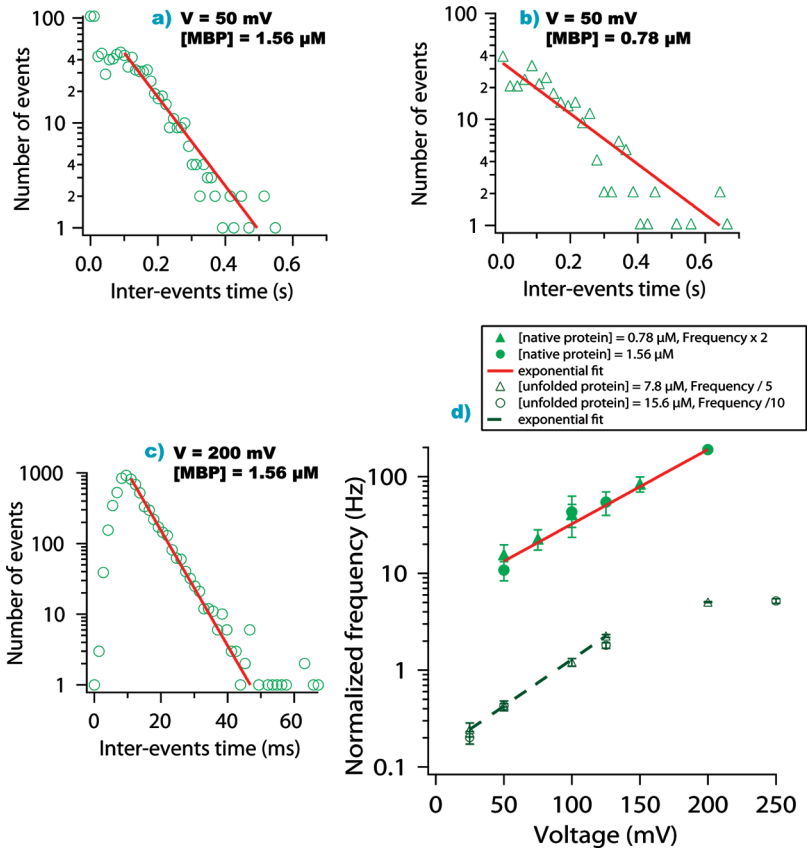

Figure 4. Normalized frequency of current blockades *versus* applied voltage in semilog scale. Explanation of the statistical analysis of the measured current traces, distribution of inter-event intervals T_i for two different protein concentrations of 1.56 μM (a) and 0.78 μM (b) with a constant voltage V = 50 and 200 mV with the same MBP concentration of 1.56 μM (c). Continuous lines are exponential fits. (d) Frequency of events *versus* applied voltage. Continuous and dotted lines are exponential fits for native and for unfolded proteins, respectively. We obtain $f = f_0\exp(|V|/V_0)$ with $f_0 = 5.5 \pm 0.5$ Hz, $V_0 = 56.4 \pm 0.5$ mV for native proteins and $f_0 = 0.14 \pm 0.01$ Hz, $V_0 = 45 \pm 0.5$ mV for unfolded proteins.

negatively charged, and in presence of KCl solution, the counterions of the nanopore are positively charged and the net charge of the protein is negatively charged. Under an applied voltage, the solvent and the protein move in opposite directions. When the ratio between the Debye length and the pore diameter is high the electro-osmotic flow magnitude is dominant, furthermore, the electro-osmotic velocity is proportional to the electrical field and we would expect that the capture would decrease when the applied voltage increases. In our experimental conditions, this is not the case: this ratio is small (0.015), and the electro-osmotic effect is not dominant. For this reason, we observe an increase of the capture when the applied voltage increases.

We also notice that the capture rate of the unfolded proteins saturates at high voltage (V >150 mV). This behavior is unusual and could be associated with a protein crowding at the entrance of the pore, due to the high electric field applied and the large protein concentration 10 times larger than the one used for folded proteins.

Analysis of the Dwell Times. We have observed that the blockade durations of the native and unfolded proteins decrease as the applied electric field increases. The measured dwell time varies between 20 $\pm$ 3 ms at 50 mV and 3.3 $\pm$ 0.7 ms at 200 mV (Figure 5d) when the proteins are in their native state, and between 3 $\pm$ 0.7 ms at 50 mV and 0.7 $\pm$ 0.1 ms at 200 mV when they are unfolded. We check that these times remain unchanged when using two different protein concentrations (Figure 5a,b).

If the electro-osmotic flow is not the dominant effect for the dynamics of protein translocation, the dwell time will be a decreasing function of the applied voltage. We observe this dependency for native or unfolded proteins.

We also find that folded proteins stay longer in the pore than unfolded ones when applying the same electric force. A possible explanation for this dwell time difference is that the interactions between the protein and the nanopore depend on the folding state of the proteins; the shape or the surface charge distribution is quite different between the folded and the unfolded conformation.

If there is no energy barrier inside the pore, the translocation time is expected to be inversely proportional to the applied force, that is, to the transmembrane

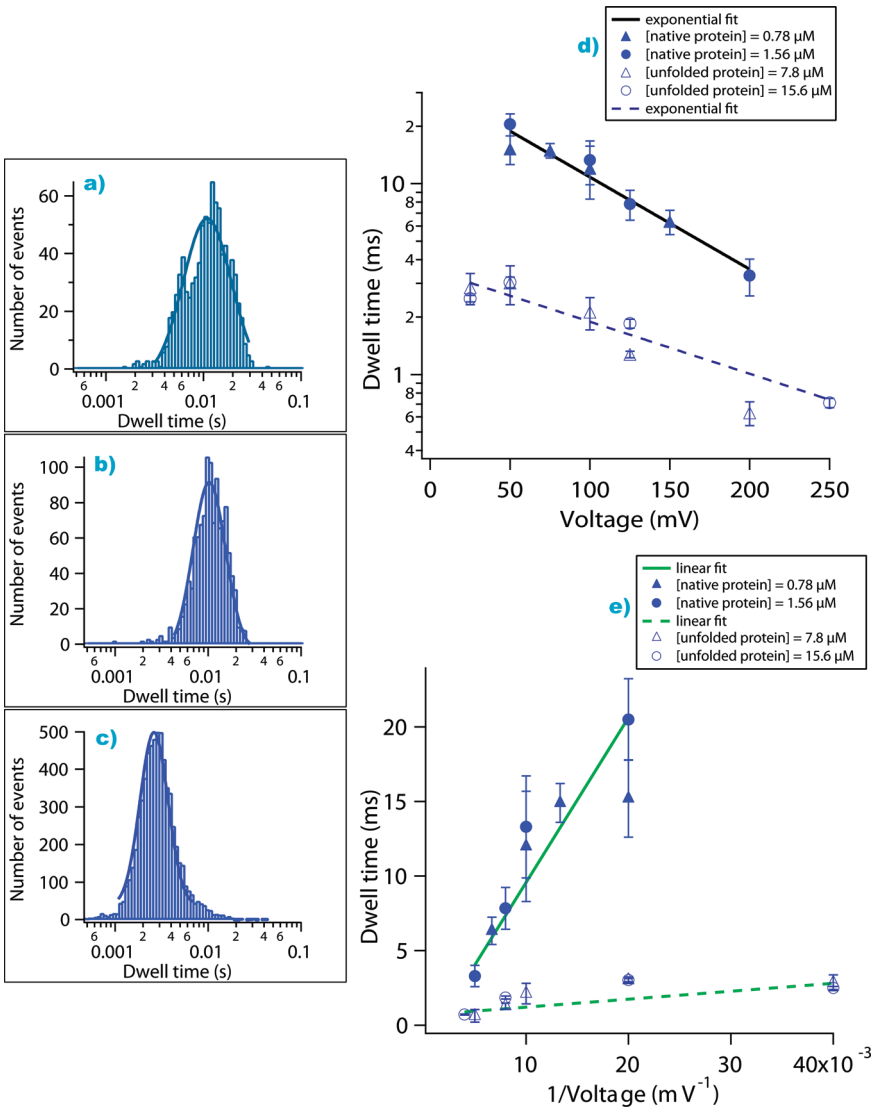

Figure 5. Dwell time of events *versus* applied voltage for native and unfolded proteins. Histograms of the dwell times for native proteins (a−c). Lines are logarithmic normal fits; the maximum of the distribution defines the most probable dwell time. MBP concentrations are (a) 0.78 and (b) 1.56 μM, and the transmembrane potential is 100 mV. (c) Protein concentration is 1.56 μM, and the applied voltage is 200 mV. Dwell time of events *versus* applied voltage; the graph is plotted on a linear scale (d) or on a semilog scale (e). The continuous line corresponds to native protein fit and the dashed line to unfolded protein fit. We find using the equation $f(V) = A\exp(-V/V_c)$: $A = 32.87 \pm 4.08$ ms, $V_c = 90.9 \pm 9.9$ mV, and $\chi^2 = 3.41$ for native proteins; $A = 3.5 \pm 0.3$ ms, $V_c = 167 \pm 33$ mV, and $\chi^2 = 1$ for unfolded proteins. Using the equation, $f(V) = b/V + a$, we obtain $a = -1.48 \pm 1.01$ ms, $b = 1104 \pm 114$ ms mV, and $\chi^2 = 9$ for native proteins and $a = 0.68 \pm 0.04$ ms, $b = 54 \pm 2.9$ ms mV, and $\chi^2 = 160$ for unfolded proteins.

voltage.[40−43] In the opposite case, translocating chains are traveling in a complex energy landscape with a well-defined energy barrier. One expects an exponential dependence of the translocation time on the applied voltage.[44] We have examined these two hypotheses by fitting the experimental data to the different predicted behaviors (Figure 5d,e). The χ^2 of the exponential and $1/V$ fit are, respectively, $\chi^2 = 3.41$ and 8.98 for the folded proteins and $\chi^2 = 1$, $\chi^2 = 160$ for the unfolded ones. The exponential dependency is clearly more convenient in both cases. This suggests that protein transport involves a free-energy barrier as observed in previous studies using protein nanopores.[15,45,46] The coupling with the electric field inside the nanopore is measured by the effective charge $z_{inside} = (k_BT)/(eV_c) = 0.28$ deduced from the voltage relationship (Figure 5e), with z_{inside} being the effective charge of the protein inside the pore. The low value of this effective charge was previously observed with DNA[47] and colloid[48] translocation using solid-state nanopores. This charge reduction is not fully explained, and it could be associated with an increased condensation of the counterions due to the confinement of the charges in the medium of low dielectric constant[49] or by the back flow effects.[38] The low values of the effective charge inside the pore are also observed with protein nanopores.[15,45,46]

In our case, the pore diameter (20 nm) is less than the membrane thickness (30 nm), the edge effects are

negligible, and the pore resistance in the first approximation is given by the Ohm law. When the pore diameter is higher than the membrane thickness, the access resistance should be given by the shape of field lines in the electrolyte at the entrance and exit of the pore and should be taken into account.[50]

As already noticed by several authors,[22−27] the durations of the observed current blockades of proteins in nanopores are anomalously long. In our case, we find values on the order of a millisecond, while one would expect transit times based on the electrophoretic mobility on the order of a microsecond. The electrophoretic velocity (v) of protein is related to the electric field strength (E) *via* $v = Q/(6\pi\eta r)E$, where Q is the protein net charge, r the protein radius, and η is the viscosity of the solution. The electrophoretic time τ_{ele} over the pore length L is $\tau_{ele} = L/v = (6\pi\eta rL)/(QE) = (6\pi\eta r)/(QL^2/V)$, where V is the applied electric voltage. In our experimental conditions, $Q = -8e$,$L = 30$ nm, $\eta = 10^{-3}$ Pa·s, at 100 mV, one estimate $\tau_{ele} = 0.2$ μs. The diffusion time through the pore length that we estimate using $\tau_{diff} = L^2/D_{diff} = (6\pi\eta r)/(k_BT)L^2 = \tau_{ele}(QV)/(k_BT)$, using the above values, is $\tau_{diff} = 6.4$ μs. These two values are certainly below the experimental measured times. This phenomenon is not yet fully understood, and several explanations have been proposed.

The first one involves attractive interactions between the proteins and the nanopore walls,[22,29] leading to protein adsorption. This is quite a common phenomenon, particularly on such a high energy surface as that of SiN.[51]

The second one, studied in detail for proteins by Firnkes *et al.*,[30] relies on the electro-osmotic effect, which may strongly slow down the passing proteins or even reverse their apparent electrophoretic mobility. The counterions of the surface charges are moved by the electrical field; they carry the solvent away with the velocity $v_s = ((\varepsilon\varepsilon_0\zeta)/(\eta))E$, where $\varepsilon = 80$ is the dielectric constant of water, $\varepsilon_0 = 8.85 \times 10^{-12}$ Fm^{-1} is the vacuum dielectric constant, and $\zeta = -10$ mV is the zeta-potential of the pore walls.[31] At KCl = 1 M and pH = 8, we find $v_s = 0.24$ ms^{-1}. In the presence of an electro-osmotic flow, the sum of electrophoretic forces and viscous friction forces is equal to zero $-|Q|(V/L) + 6\pi\eta r(v_s - v) = 0$, where v_s and v are, respectively, the solvent and protein velocity. With our values, we find $v = v_s - |Q|(V/(6\pi\eta rL)) = 0.24 - 0.11 = 0.13$ ms^{-1}. This velocity is positive, which means that the protein should never enter into the pore, which contradicts our experimental results. Recently, it has been shown that electro-osmotic velocity is also controlled by the geometry and diameter of the pore.[38,39] In our experimental conditions, the ratio between the Debye length (3 Å) and the surface separation (pore diameter: 200 Å) is small (0.015), and the electro-osmotic flow magnitude is reduced; this is a possible explanation of why the proteins still enter the nanopores.

In our case, we observe significant frequency of current blockades, and the number of events increases with applied voltage.

In order to discuss the possible explanations for the anomalous dynamics for protein transport through a nanopore, we evaluate the blockade frequency for purely Brownian diffusion proteins. The equation used below is valid for a perfect disk; this is not the case with the solid-state nanopore used in our experiment. However, by using the equation below, we evaluate the events frequency magnitude for a purely Brownian diffusion.[52] The blockade frequency is given by $f = 2\pi D_{diff}cr_{pore} = (k_BTc)/(3\eta)r_{pore}/r$, where $D_{diff} = (k_BT)/(6\pi\eta r)$ is the self-diffusion coefficient for isolated Brownian proteins (Stokes−Einstein equation), c is the protein concentration, and r_{pore} and r are the pore and protein radii, respectively. For 1 μM protein concentration, we find a frequency, $f = 4000$ Hz. This value is 2 orders of magnitude higher than the measured frequency. This predicted value suggests that either the proteins adsorbed on the pore walls or there are missed events. Regarding the missed events, it was shown by Winterhalter and his colleagues[53] for the transport of antibiotics through membrane channels that the dwell times of the antibiotics inside the channel decrease strongly with an increase in temperature. Consequently, the fast translocation events are probably not visible, due to the limited resolution of the instrument. In the future, the resolution of the current measurement will need to be significantly increased to be able to resolve the events.[54] Events could be canceled by the electro-osmotic flow or by the potential barrier. The third one, more subtle, is based on the heterogeneity in the charge distribution all along the protein,[22] leading to a disordered energy landscape as the protein threads through a pore. A supplementary source of complication is that protein adsorption interferes with the electro-osmotic and the energy landscape effects, by changing the surface charge of the pore, hindering motion of the counterions close to the surface and modifying the interactions between the pore and the proteins.[55]

Double MalE. We have investigated the effect of the pore diameter dependence on the current blockade, normalized current blockade, and dwell time for completely unfolded proteins. We use a double MBP (Figure 6 left) and a single MBP (Figure 6 right) with two different pore diameters, 4 and 20 nm, respectively (Figure 6). We observe that the width of events (the dwell time) and the current blockade magnitude are more significant using the smaller pore size (Figure 6a,b). From the current traces, we expect the ratio I_{4nm}/I_{20nm} to vary as $(D_{4nm}/D_{20nm})^2$, where I_{4nm}, I_{20nm}, D_{4nm}, and D_{20nm} are the mean currents of open pores and pore diameters corresponding to 4 and 20 nm. The estimated value $(D_{4nm}/D_{20nm})^2 = 0.040$ is similar to that

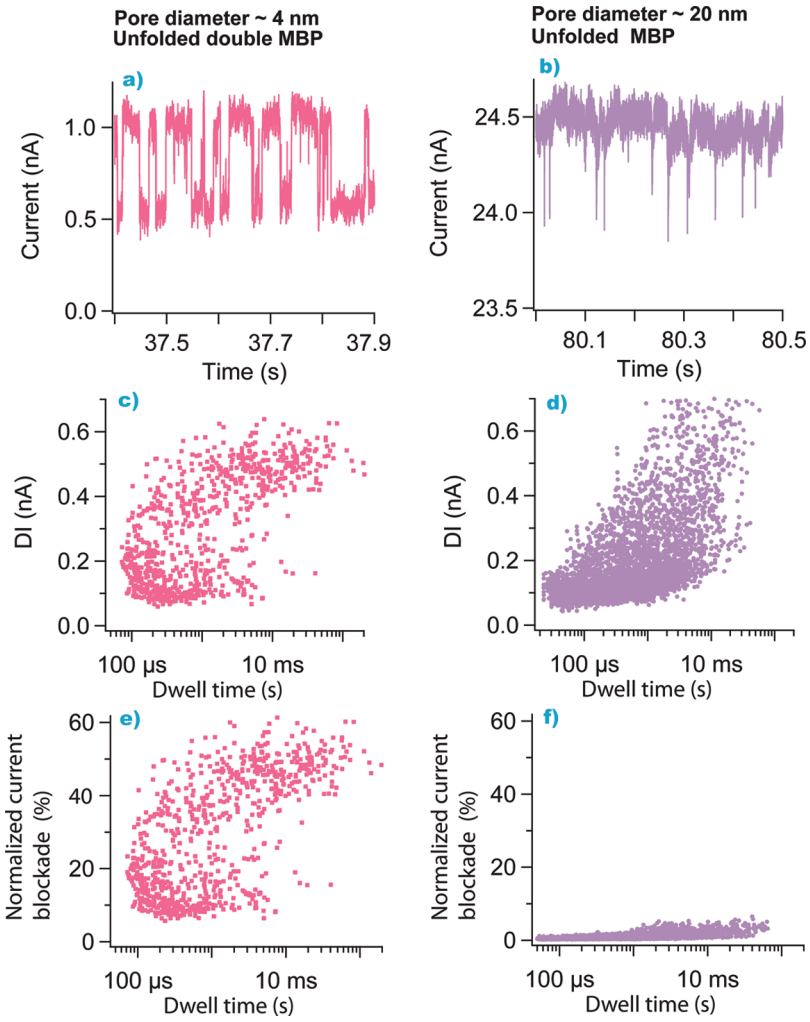

Figure 6. Electrical characterization of protein and nanopore size effets. Transport of unfolded double MBP protein (left) and single MBP protein (right) through two different pore diameters, 4 nm (a,c,e) and 20 nm (b,d,f), respectively. Detail of a current trace in the presence of (a) unfolded double MBP (15.6 μM) or (b) single MBP (7.8 μM) through a solid-state nanopore. In both traces, the applied voltage is 150 mV. Event scatter plot of dwell time *versus* current blockade, respectively, for double unfolded protein (c) and single unfolded protein (d). Event scatter plot of dwell time *versus* normalized current blockade (%) for double unfolded MBP (e) and single unfolded MBP protein (f).

obtained I_{4nm}/I_{20nm} = 1.04/24.47 = 0.042, suggesting that currents of open pores are consistent with pore sizes. This result also shows the presence of unfolded proteins inside the pore. Short events are associated with low current blockades, and long events are correlated to high current blockades (Figure 6c,d). The duration of short and long events of single unfolded proteins are shifted toward the lower values compared to double unfolded proteins. In order to compare the blockade rate caused by unfolded proteins through 4 and 20 nm pores, we represent a diagram of percentage of the normalized current blockade *versus* dwell time (Figure 6e,f). We observe that the normalized blockade of long events increases as the pore size decreases from 4 to 20 nm. The measured value for the percentage of the normalized current blockade of unfolded proteins through a 4 nm pore is 30−60% *versus* 0.5−2% through a 20 nm pore.

In conclusion, we compare the transport of native and unfolded proteins through solid-state nanopores drilled by FIB, and we observe anomalous protein translocation dynamics. In our experimental conditions, we show that this dynamic is associated with a free-energy barrier. The capture rate increases exponentially as a function of applied voltage, and the dwell time decreases exponentially when the electrical force increases. The unfolded protein is partially stretched under the electrical field. The capture rate of unfolded proteins is lower than that of native proteins and saturates at high voltage. The dwell time of proteins is very long, and compact native proteins stay longer in the pore than unfolded ones. In the future, we will investigate the origin of anomalous dynamics observed for native and unfolded proteins. In order to separate the electro-osmotic effect from protein−pore interaction effects or crowding effects, we plan to

perform experiments at different net charges, for either the proteins and the pores and with different polypeptide chain lengths. We will also examine the high applied voltage regime and study the translocation through a solid-state nanopore with a narrow pore diameter.

METHODS

Solid-State Nanopores. In order to fabricate solid-state nanopores, we used standard free-standing Si_3N_4 membranes (Protochips Inc.). Nanopores were drilled in 30 nm membranes as previously described[56] using a focused ion beam instrument. This very high resolution FIB is especially suitable for the reproducible fabrication of nanometer sized pores.[11,56] In contrast with the usual nanodrilling technique based on the TEM local heating technique, the ion interaction process allows the ion dose to be calibrated precisely in one step, for irradiation times ranging between 10 ms and some hundreds of milliseconds.[56] In this study, we have chosen a medium ion dose (750 ms/pt) in order to fabricate nanopores with diameters from 4 to 20 nm. All of the nanopores were adapted to an easy-to-use "Port-a-patch" setup (Nanion Technologies Gmbh). They were glued onto a drilled screw cap containing a 1−2 mm wide hole. This chip can be easily manipulated and rinsed with water and ethanol. In order to make the membrane hydrophilic, we cleaned this chip by exposing each side to oxygen plasma for 2 min. We then put a 10 μL buffer droplet on each side of the nanopore using a micropipet. The buffer was an ionic solution of 1 M KCl containing 5 mM Tris (pH 7.5) and allowed good storage conditions. The experiments were conducted in a water-saturated atmosphere. The effective pore diameter was deduced from an open-pore conductance measurement assuming a cylindrical shape. The denaturing agent (guanidium-HCl) did not affect the noise level and pore stability. Addition of guanidium-HCl increased only the ionic current of the open pore.

Proteins. The recombinant maltose binding protein (MBP or MalE) of *Escherichia coli* contained 370 residues (M_r = 40 707) and was negatively charged (with a net charge $Z = -8e$) at physiological pH. The wild-type MBP was purified as described.[57] The tandem protein, MalE−MalE or double MBP, was constructed by subcloning a PCR-amplified DNA fragment of the corresponding mature sequence of MalE with primers containing a *Hin*dIII adaptor as described.[15] The buffer was an ionic solution of 1 M KCl containing 5 mM Tris (pH 7.5). In this study, we added to this ionic solution the single or double recombinant MBP denatured by guanidium chloride (Gdm-HCl). The final concentration of guanidium chloride used was 1.44 M.

Data Acquisition. The ionic currents were detected using an Axopatch 200B amplifier (Molecular Devices). They were first filtered at 10 kHz before a digitization at 250 kHz. The data were processed with a homemade macro using Igor software (Wavemetrics). The event measurements were based on a statistical analysis of the current traces. The statistical analysis of the current traces have been previously described.[45] This method was based on a two thresholds method, in the case of events with asymmetric shape; the event duration was function of the threshold. As our threshold criterion was always the same, and the measurement error was constant and remained low. All data were obtained with a single nanopore, but for each experimental condition, we measured at least 2000 events. The same nanopore was used during several experiments and several days with the MalE. The physical parameters were estimated without the standard deviation between different pores but with the standard deviation of several assays with the same pore. Another pore of different size was used during the experiments with the double MalE. Data were systematically checked for reproducibility.

Acknowledgment. This work was supported by a grant funding, Action Thématique Incitative Génopole, ANR Blanche "TRANSFOLDPROT" BLAN08-1_339991 and by ANR "ACTIVE NANOPORES" No. ANR-06-NANO-028 by Nanoscience Eranet, ANR "NANOPORE" No. 08-NSCI-006-01. We are grateful to Kari and Damien Foster for their attention to our manuscript and for kindly correcting the language of the manuscript.

REFERENCES AND NOTES

1. Dekker, C. Solid-State Nanopores. *Nat. Nanotechnol.* **2007,** *2*, 209–215.
2. Howorka, S.; Siwy, Z. S. Nanopore Analytics: Sensing of Single Molecules. *Chem. Soc. Rev.* **2009,** *38*, 2360–2384.
3. Kasianowicz, J. J.; Brandin, E.; Branton, D.; Deamer, D. W. Characterization of Individual Polynucleotide Molecules Using a Membrane Channel. *Proc. Natl. Acad. Sci. U.S.A.* **1996,** *93*, 13770–13773.
4. Kasianowicz, J. J.; Robertson, J. W. F.; Chan, E. R.; Reiner, J. E.; Stanford, V. M. Nanoscopic Porous Sensors. *Annu. Rev. Anal. Chem.* **2008,** *1*, 737.
5. Movileanu, L. Interrogating Single Proteins through Nanopores: Challenges and Opportunities. *Trends Biotechnol.* **2009,** *27*, 333–341.
6. Muthukumar, M. Mechanism of DNA Transport through Pores. *Annu. Rev. Biophys. Biomol. Struct.* **2007,** *36*, 435–450.
7. Branton, D.; Deamer, D. W.; Marziali, A.; Bayley, H.; Benner, S. A.; Butler, T.; Di Ventra, M.; Garaj, S.; Hibbs, A.; Huang, X.; *et al.* The Potential and Challenges of Nanopore Sequencing. *Nat. Biotechnol.* **2008,** *26*, 1146–1153.
8. Reiner, J. E.; Kasianowicz, J. J.; Nablo, B. J.; Robertson, J. W. F. Theory for Polymer Analysis Using Nanopore-Based Single-Molecule Mass Spectrometry. *Proc. Natl. Acad. Sci. U.S. A.* **2010,** *107*, 12080–12085.
9. Zimmerberg, J.; Parsegian, V. A. Polymer Inaccessible Volume Changes during Opening and Closing of a Voltage-Dependent Ionic Channel. *Nature* **1986,** *323*, 36–39.
10. Bayley, H.; Cremer, P. S. Stochastic Sensors Inspired by Biology. *Nature* **2001,** *413*, 226–230.
11. Li, J.; Stein, D.; McMullan, C.; Branton, D.; Aziz, M. J.; Golovchenko, J. A. Ion-Beam Sculpting at Nanometre Length Scales. *Nature* **2001,** *412*, 166–169.
12. He, Y.; Gillespie, D.; Boda, D.; Vlassiouk, I.; Eisenberg, R. S.; Siwy, Z. S. Tuning Transport Properties of Nanofluidic Devices with Local Charge Inversion. *J. Am. Chem. Soc.* **2009,** *131*, 5194–5202.
13. Rapoport, T. A. Protein Translocation Across the Eukaryotic Endoplasmic Reticulum and Bacterial Plasma Membranes. *Nature* **2007,** *450*, 663–669.
14. Oukhaled, G.; Mathe, J.; Biance, A. L.; Bacri, L.; Betton, J. M.; Lairez, D.; Pelta, J.; Auvray, L. Unfolding of Proteins and Long Transient Conformations Detected by Single Nanopore Recording. *Phys. Rev. Lett.* **2007,** *98*, 158101–158104.
15. Pastoriza-Gallego, M.; Rabah, L.; Gibrat, G.; Thiebot, B.; van der Goot, F. G.; Auvray, L.; Betton, J. M.; Pelta, J. Dynamics of Unfolded Protein Transport through an Aerolysin Pore. *J. Am. Chem. Soc.* **2011,** *133*, 2923–2931.
16. Baran, C.; Smith, G. S. T.; Bamm, V. V.; Harauz, G.; Lee, J. S. Divalent Cations Induce a Compaction of Intrinsically Disordered Myelin Basic Protein. *Biochem. Biophy. Res. Commun.* **2010,** *391*, 224–229.
17. Pastoriza-Gallego, M.; Gibrat, G.; Thiebot, B.; Betton, J. M.; Pelta, J. Polyelectrolyte and Unfolded Protein Pore Entrance Depends on the Pore Geometry. *Biochim. Biophys. Acta* **2009,** *1788*, 1377–1386.
18. Stefureac, R.; Waldner, L.; Howard, P.; Lee, J. S. Nanopore Analysis of a Small 86-Residue Protein. *Small* **2008,** *4*, 59–63.

19. Sutherland, T. C.; Long, Y. T.; Stefureac, R. I.; Bediako-Amoa, I.; Kraatz, H. B.; Lee, J. S. Structure of Peptides Investigated by Nanopore Analysis. *Nano Lett.* **2004,** *4*, 1273–1277.
20. Lesieur, C.; Frutiger, S.; Hughes, G.; Kellner, R.; Pattus, F.; van der Goot, F. G. Increased Stability upon Heptamerization of the Pore-Forming Toxin Aerolysin. *J. Biol. Chem.* **1999,** *274*, 36722–36728.
21. Pastoriza-Gallego, M.; Oukhaled, G.; Mathe, J.; Thiebot, B.; Betton, J. M.; Auvray, L.; Pelta, J. Urea Denaturation of α-Hemolysin Pore Inserted in Planar Lipid Bilayer Detected by Single Nanopore Recording: Loss of Structural Asymmetry. *FEBS Lett.* **2007,** *581*, 3371–3376.
22. Talaga, D. S.; Li, J. Single-Molecule Protein Unfolding in Solid State Nanopores. *J. Am. Chem. Soc.* **2009,** *131*, 9287–9297.
23. Fologea, D.; Ledden, B.; McNabb, D. S.;Li, J. Electrical Characterization of Protein Molecules by a Solid-State Nanopore. *Appl. Phys. Lett.* 2007, *91*, nihpa38991.
24. Han, A.; Schurmann, G.; Mondin, G.; Bitterli, R. A.; Hegelbach, N. G.; de Rooij, N. F.; Staufer, U. Sensing Protein Molecules Using Nanofabricated Pores. *Appl. Phys. Lett.* **2006,** *88*, 093901–093903.
25. Han, A.; Creus, M.; Schuêrmann, G.; Linder, V.; Ward, T. R.; de Rooij, N. F.; Staufer, U. Label-Free Detection of Single Protein Molecules and Protein−Protein Interactions Using Synthetic Nanopores. *Anal. Chem.* **2008,** *80*, 4651–4658.
26. Sexton, L. T.; Horne, L. P.; Sherrill, S. A.; Bishop, G. W.; Baker, L. A.; Martin, C. R. Resistive-Pulse Studies of Proteins and Protein/Antibody Complexes Using a Conical Nanotube Sensor. *J. Am. Chem. Soc.* **2007,** *129*, 13144–13152.
27. Sexton, L. T.; Mukaibo, H.; Katira, P.; Hess, H.; Sherrill, S. A.; Horne, L. P.; Martin, C. R. An Adsorption-Based Model for Pulse Duration in Resistive-Pulse Protein Sensing. *J. Am. Chem. Soc.* **2010,** *132*, 6755–6763.
28. Wanunu, M.; Sutin, J.; McNally, B.; Chow, A.; Meller, A. DNA Translocation Governed by Interactions with Solid-State Nanopores. *Biophys. J.* **2008,** *95*, 4716–4725.
29. Niedzwiecki, D. J.; Grazul, J.; Movileanu, L. Single-Molecule Observation of Protein Adsorption onto an Inorganic Surface. *J. Am. Chem. Soc.* **2010,** *132*, 10816–10822.
30. Stefureac, R. I.; Trivedi, D.; Marziali, A.; Lee, J. S. Evidence That Small Proteins Translocate through Silicon Nitride Pores in a Folded Conformation. *J. Phys.: Condens. Matter.* **2010,** *22*, 450301.
31. Firnkes, M.; Pedone, D.; Knezevic, J.; Doblinger, M.; Rant, U. Electrically Facilitated Translocations of Proteins through Silicon Nitride Nanopores: Conjoint and Competitive Action of Diffusion, Electrophoresis, and Electroosmosis. *Nano Lett.* **2010,** *10*, 2162–2167.
32. Betton, J. M.; Hofnung, M. Folding of a Mutant Maltose-Binding Protein of *Escherichia coli* which Forms Inclusion Bodies. *J. Biol. Chem.* **1996,** *271*, 8046–8052.
33. Spurlino, J. C.; Lu, G. Y.; Quiocho, F. A. The 2.3-A Resolution Structure of the Maltose- or Maltodextrin-Binding Protein, a Primary Receptor of Bacterial Active Transport and Chemotaxis. *J. Biol. Chem.* **1991,** *266*, 5202–5219.
34. Brendel, V.; Bucher, P.; Nourbakhsh, I. R.; Blaisdell, B. E.; Karlin, S. Methods and Algorithms for Statistical Analysis of Protein Sequences. *Proc. Natl. Acad. Sci. U.S.A.* **1992,** *89*, 2002–2006.
35. Lairez, D.; Pauthe, E.; Pelta, J. Refolding of a High Molecular Weight Protein: Salt Effect on Collapse. *Biophys. J.* **2003,** *84*, 3904–3916.
36. Henrickson, S. E.; Misakian, M.; Robertson, B.; Kasianowicz, J. J. Driven DNA Transport into an Asymmetric Nanometer-Scale Pore. *Phys. Rev. Lett.* **2000,** *85*, 3057–3060.
37. Storm, A. J.; Storm, C.; Chen, J.; Zandbergen, H.; Joanny, J. F.; Dekker, C. Fast DNA Translocation through a Solid-State Nanopore. *Nano Lett.* **2005,** *5*, 1193–1197.
38. Keyser, U. F.; van Dorp, S.; Lemay, S. G. Tether Forces in DNA Electrophoresis. *Chem. Soc. Rev.* **2010,** *39*, 939–947.
39. van Dorp, S.; Keyser, U. F.; Dekker, N. H.; Dekker, C.; Lemay, S. G. Origin of the Electrophoretic Force on DNA in Solid-State Nanopores. *Nat. Phys.* **2009,** *5*, 347–351.
40. Reguera, D.; Schmid, G.; Burada, P. S.; Rubi, J. M.; Reimann, P.; Hanggi, P. Entropic Transport: Kinetics, Scaling, and Control Mechanisms. *Phys. Rev. Lett.* **2006,** *96*, 130603.
41. Kantor, Y.; Kardar, M. Anomalous Dynamics of Forced Translocation. *Phys. Rev. E* **2004,** *69*, 021806.
42. Slonkina, E.; Kolomeisky, A. B. Polymer Translocation through a Long Nanopore. *J. Chem. Phys.* **2003,** *118*, 7112–7118.
43. Sung, W.; Park, P. J. Polymer Translocation through a Pore in a Membrane. *Phys. Rev. Lett.* **1996,** *77*, 783–786.
44. Hanggi, P.; Talkner, P.; Borkovec, M. Reaction-Rate Theory: Fifty Years after Kramers. *Rev. Mod. Phys.* **1990,** *62*, 251.
45. Brun, L.; Pastoriza-Gallego, M.; Oukhaled, G.; Mathe, J.; Bacri, L.; Auvray, L.; Pelta, J. Dynamics of Polyelectrolyte Transport through a Protein Channel as a Function of Applied Voltage. *Phys. Rev. Lett.* **2008,** *100*, 158302–158304.
46. Gibrat, G.; Pastoriza-Gallego, M.; Thiebot, B.; Breton, M. F.; Auvray, L.; Pelta, J. Polyelectrolyte Entry and Transport through an Asymmetric α-Hemolysin Channel. *J. Phys. Chem. B* **2008,** *112*, 14687–14691.
47. Smeets, R. M. M.; Keyser, U. F.; Krapf, D.; Wu, M. Y.; Dekker, N. H.; Dekker, C. Salt Dependence of Ion Transport and DNA Translocation through Solid-State Nanopores. *Nano Lett.* **2006,** *6*, 89–95.
48. Bacri, L.; Oukhaled, A. G.; Schiedt, B.; Patriarche, G.; Bourhis, E.; Gierak, J.; Pelta, J.; Auvray, L. Dynamics of Colloids in Single Solid-State Nanopores. *J. Phys. Chem. B* **2011,** *115*, 2890–2898.
49. Zhang, J. S.; Shklovskii, B. I. Effective Charge and Free Energy of DNA inside an Ion Channel. *Phys. Rev. E.* **2007,** *75*, 021906.
50. Hall, J. E. Access Resistance of a Small Circular Pore. *J. Gen. Physiol.* **1975,** *66*, 531–532.
51. Roach, P.; Farrar, D.; Perry, C. C. Interpretation of Protein Adsorption: Surface-Induced Conformational Changes. *J. Am. Chem. Soc.* **2005,** *127*, 8168–8173.
52. Wanunu, M.; Morrison, W.; Rabin, Y.; Grosberg, A. Y.; Meller, A. Electrostatic Focusing of Unlabelled DNA into Nanoscale Pores Using a Salt Gradient. *Nat. Nanotechnol.* **2010,** *5*, 160–165.
53. Mahendran, K. R.; Chimerel, C.; Mach, T.; Winterhalter, M. Antibiotic Translocation through Membrane Channels: Temperature-Dependent Ion Current Fluctuation for Catching the Fast Events. *Eur. Biophys. J. Biophys. Lett.* **2009,** *38*, 1141–1145.
54. Tabard-Cossa, V.; Trivedi, D.; Wiggin, M.; Jetha, N. N.; Marziali, A. Noise Analysis and Reduction in Solid-State Nanopores. *Nanotechnology* **2007,** *18*, 305505.
55. Pedone, D.; Firnkes, M.; Rant, U. Data Analysis of Translocation Events in Nanopore Experiments. *Anal. Chem.* **2009,** *81*, 9689–9694.
56. Schiedt, B.; Auvray, L.; Bacri, L.; Oukhaled, G.; Madouri, A.; Bourhis, E.; Patriarche, G.; Pelta, J.; Jede, R.; Gierak, J. Direct FIB Fabrication and Integration of "Single Nanopore Devices" for the Manipulation of Macromolecules. *Microelectron. Eng.* **2010,** *87*, 1300–1303.
57. Arie, J. P.; Miot, M.; Sassoon, N.; Betton, J. M. Formation of Active Inclusion Bodies in the Periplasm of *Escherichia coli*. *Mol. Microbiol.* **2006,** *62*, 427–437.